

Spontaneous improvement of spatial coherence and frequency locking in high-pump-power multimode lasers

F. Papoff

Department of Physics, University of Strathclyde, 107 Rottenrow, Glasgow G4 0NG, Scotland, United Kingdom

G. D'Alessandro

School of Mathematics, University of Southampton, Southampton SO17 1BJ, England, United Kingdom

(Received 16 August 2004; published 10 December 2004)

By using the time average of amplitude products we are able to identify changes in the dynamical complexity and the spatial coherence of a multimode laser. We find that there are cases in which as the pump increases, the dynamical complexity decreases and the spatial coherence improves. In some limiting cases the complexity is reduced to zero and the beam is completely coherent spatially. We show that these phenomena are caused by phase synchronization of the mode amplitudes and that they can be observed using slow detectors.

DOI: 10.1103/PhysRevA.70.063805

PACS number(s): 42.60.Jf, 42.65.Sf, 42.55.Ah, 05.45.Xt

I. INTRODUCTION

Multimode laser dynamics is the result of a complex interplay between the cavity modes, whose nature is fixed solely by the optical cavity and its symmetries, and the interaction with the active medium. It is possible to study in detail the case of few-mode dynamics or modes with some degeneracies (see, for example, [1] for a review of the two-mode case or [2] for a study of the antiphase dynamics of N identical modes). However, when the number of modes increases analytical treatments become scarce and one is forced to revert to average methods.

In a recent paper [3] we have discussed in detail the deductions on the nature of multimode laser dynamics that can be inferred by the observation of the symmetries of average intensity patterns. Average intensity patterns are the aspect of laser dynamics that can be most easily measured as by definition they require only slow detectors. Here we focus on techniques to study the nature of multimode laser dynamics that are based on an appropriate entropy introduced in [4] and developed here in the context of multimode laser dynamics. These are more powerful and give a deeper insight than average intensity patterns, but also require more experimental effort in order to be measured. The most startling result of the entropy analysis is that the complexity of the laser dynamics is not necessarily a monotonic function of the pump power: it is quite possible for the complexity first to increase and then to decrease as a function of the pump power. From a practical point of view, the key point is that the spatial coherence of the laser beam improves when its complexity decreases. This is the situation corresponding to the regular patterns of [5,6,7], but also of irregular nonsymmetric patterns that do not fit in the classification scheme devised in [5]. Moreover, this behavior is very similar to what happens when only two cavity modes are active [1]: the solution with lowest threshold is the single-mode solution (low complexity); this loses stability to a periodic solution that involves both cavity modes (high complexity), which is replaced, as the pump is increased further, by a stationary mode-locked solution (low complexity).

The structure of this paper is as follows: in the next section we introduce the biorthogonal decomposition [8] and

use it to define a statistical entropy that we use in Sec. III to study the dynamics of the multimode laser whose model was developed in Ref. [3].

II. THE BIORTHOGONAL DECOMPOSITION

A. Introduction

Roughly, the biorthogonal decomposition [4,8–10] represents a given space-time function (in the case of this paper the amplitude of the electric field in the laser cavity) in terms of independent functions of space and time only. In other words, it identifies the linearly independent components in space *and* in time that underly a given signal.

Here we summarize the main ideas of the biorthogonal decomposition using a notation suitable for complex fields. Let $X \subseteq \mathbb{R}^n$ and $T \subset \mathbb{R}$ and $H(X)$ and $H(T)$ are Hilbert spaces on X and T , respectively, each endowed with an inner product, $(\cdot, \cdot)_{X,T}$, respectively. Given a function $u(\mathbf{x}, t) \in H(XT)$, we define the operator U from $H(X)$ to $H(T)$ as

$$\forall \varphi \in H(X), \quad (U\varphi)(t) = (u, \varphi)_X \equiv \int_X \overline{u(\mathbf{x}, t)} \varphi(\mathbf{x}) d\mathbf{x}. \quad (1)$$

The adjoint of U is

$$\forall \psi \in H(T), \quad (U^* \psi)(\mathbf{x}) = (\bar{u}, \psi)_T \equiv \int_T u(\mathbf{x}, t) \psi(t) dt. \quad (2)$$

Since U acts from one Hilbert space to another one the equation $U\varphi = \lambda\psi$ is insufficient to determine the eigenvectors of U . They are given by the simultaneous equations

$$U\varphi = \lambda\psi, \quad U^* \psi = \lambda\varphi, \quad (3)$$

or, equivalently, in terms of the Hermitian operator V acting on the space $H(X) \oplus H(T)$,

$$V \begin{pmatrix} \varphi \\ \psi \end{pmatrix} = \begin{pmatrix} 0 & U^* \\ U & 0 \end{pmatrix} \begin{pmatrix} \varphi \\ \psi \end{pmatrix} = \lambda \begin{pmatrix} \varphi \\ \psi \end{pmatrix}. \quad (4)$$

The eigenvectors $\varphi(\mathbf{x})$ and $\psi(t)$ are called *topos* and *chronos*, respectively. They form sets of orthogonal functions φ_n in $H(X)$, ψ_n in $H(T)$, and $(\varphi_n, \psi_n)^T$ in $H(X) \oplus H(T)$, and thus identify the linearly independent components of the space-time function $u(\mathbf{x}, t)$. If U is a compact operator then there are countably many topos and chronos and we can decompose the function $u(\mathbf{x}, t)$ as

$$u(\mathbf{x}, t) = \sum_n \lambda_n \varphi_n(\mathbf{x}) \bar{\psi}_n(t), \quad (5)$$

with $\lambda_1 \geq \lambda_2 \geq \dots > 0$. This expression is called the biorthogonal decomposition of the function $u(\mathbf{x}, t)$.

The orthonormality of the $\bar{\psi}_n(t)$ means that the average intensity pattern is a linear superposition of the intensities of the topos,

$$\langle |u|^2 \rangle_{\tau_0} = \sum_n \lambda_n^2 |\varphi_n(\mathbf{x})|^2, \quad (6)$$

where $\langle \cdot \rangle_{\tau_0} \equiv (\cdot, \cdot)_{T/\tau_0}$ indicates the average in time over the length τ_0 of the interval $T \subset \mathbb{R}$. By suitably normalizing the topos so that $(\varphi_n, \varphi_m)_X = \delta_{nm}$ we can see from Eq. (6) that the coefficients λ_n^2 are a measure of how much of the “energy” of the function $u(\mathbf{x}, t)$ is accounted for by the pair $\{\varphi_n(\mathbf{x}), \psi_n(t)\}$. We can therefore use the eigenvalues of the decomposition (5) to define the entropy [4]:

$$H = - \sum_n p_n \log p_n, \quad (7)$$

where $p_n = \lambda_n^2 / \sum_i \lambda_i^2$ is the normalized eigenvalue. The value of the entropy is an indication of the spreading of the energy over the topos. Its maximum value is $H = \log(M)$, with M the number of topos with eigenvalue different from zero, and corresponds to equipartition of energy over M topos. Its minimum value is $H = 0$, when only one eigenvalue is different from zero and all the energy is concentrated in a single topos. Equation (7) can be written in operator form as

$$H = - \text{Tr} \left[\frac{\mathcal{U}}{\text{Tr}(\mathcal{U})} \log \left(\frac{\mathcal{U}}{\text{Tr}(\mathcal{U})} \right) \right], \quad (8)$$

where $\mathcal{U} \equiv U^* U$ is the two-point spatial correlation operator. This shows that the entropy defined by Eq. (7) is formally a von Neumann-type entropy [11] where the operator $\mathcal{U}/\text{Tr}(\mathcal{U})$ plays the role of the density matrix. The spectrum of \mathcal{U} and H clearly indicate how many independent “coherent” structures there are and how the energy is distributed over these structures. For lasers, this is related to the spatial coherence of the beam. For instance, for $H = 0$ the dynamics of the laser may be chaotic, but the beam is spatially coherent. In general, when H is higher, the spatial coherence of the beam is lower.

Moreover, note that V , \mathcal{U} , and $U^* \equiv U U^*$ have the symmetry of their kernels. Therefore, as the control parameters are changed, the symmetry and the eigenvalue spectra of these operators are expected to change. This is the most useful aspect of this technique, in that it allows us to detect bifurcations of the dynamics and of the spatial and temporal correlations of the system through the changes of value and degeneracy of the eigenvalues of these operators.

B. The biorthogonal decomposition and laser dynamics

We consider the following model for a two-level ring laser [3]:

$$\frac{\partial F}{\partial t} = \mathcal{L}F + P, \quad (9)$$

$$\frac{\partial P}{\partial t} = -P + \chi F + FN, \quad (10)$$

$$\frac{\partial N}{\partial t} = -\gamma \left[N + \frac{1}{2}(F\bar{P} + \bar{F}P) \right], \quad (11)$$

where \mathcal{L} is a linear spatial propagation operator that depends on the cavity geometry through its $ABCD$ matrices [12], F and P are the slowly varying amplitudes of the electric field and polarization, respectively, while N is the population inversion. γ is the ratio between the decay times of the polarization and of the population inversion and χ is the pump parameter. This model has been analyzed in detail in [3] where it has been found in good agreement with experimental results. Its main strengths are that it is possible to include hard apertures in the modeling of the cavity and that we can study both class C and class B lasers for high pump values without approximations. We consider here regimes in which there is a number M of cavity modes above the lasing threshold. Therefore, for any given value of t and x , F is contained in a finite-dimensional subspace $H_F(X) \subset H(X)$ and $H_F(T) \subset H(T)$, respectively. In these circumstances it becomes very convenient to use the modal decomposition

$$F(\mathbf{x}, t) = \sum_{k=1}^M \bar{f}_k(t) A_k(\mathbf{x}), \quad (12)$$

where the cavity modes $A_k(\mathbf{x})$ are the eigenfunctions of the linear operator \mathcal{L} and $\bar{f}_k(t)$ are their amplitudes.

One of the key results of [3] is that the time average of the products of the amplitudes of the cavity modes is not always negligible. In general one has

$$\langle |F|^2 \rangle_{\tau_0} = \sum_{j,k=1}^M \langle f_j \bar{f}_k \rangle_{\tau_0} \bar{A}_j(\mathbf{x}) A_k(\mathbf{x}), \quad (13)$$

where the length τ_0 of the averaging interval $T \subset \mathbb{R}$ is much longer than the natural time scale of the laser. In [5,6] it was found that some regular patterns can be very well approximated by the superposition of the intensity of the cavity modes, i.e., they are consistent with the hypothesis that in Eq. (13) $\langle f_j \bar{f}_k \rangle_{\tau_0} = \delta_{jk} C_k$, where $\{C_k\}$ are normalization factors. However, in Ref. [3] it was shown that in general the average amplitude products are not zero and that they have macroscopic effects, in the sense that they may alter the symmetry of the average intensity patterns. Here we show that they give rise to spatiotemporal coherent structures, the topos and chronos of the laser dynamics, and that, ultimately, they may considerably reduce the complexity of the laser dynamics at high pump powers.

Using the notation of Sec. II A we identify the (smooth) function $u(\mathbf{x}, t)$ with the electric field amplitude $F(\mathbf{x}, t)$, the Hilbert spaces $H(X)$ and $H(T)$ with $L_2(\mathbb{R}^2)$ and $L_2([0, \tau_0])$, respectively. The topos and chronos of the laser dynamics are given by solving the eigenvalue problem (3). It is also possible to compute the topos as the eigenfunctions of the two-point spatial correlation operator $\mathcal{U} \equiv U^* U$:

$$\mathcal{U}\varphi \equiv U^* U\varphi = \int_T F(\mathbf{x}, t) \int_X \bar{F}(\mathbf{x}', t) \varphi(\mathbf{x}') dx' dt = \lambda^2 \varphi. \quad (14)$$

The chronos must then be obtained by projecting the electric field F on the topos.¹ If one uses this procedure with topos obtained for a given set of control parameter values to another set, the temporal functions obtained will not be, in general, orthogonal in time. We will use this property later to discuss the nature of the bifurcations of the system.

C. Relation between topos and the cavity modes

In order to apply the general theory of the previous sections to a specific problem, we need to find the appropriate basis to represent the operators V and \mathcal{U} . In laser physics the cavity modes and their amplitudes form the most natural bases. The cavity modes $A_k(\mathbf{x})$ are the eigenfunctions of the linear evolution operator \mathcal{L} of Eq. (9): $\mathcal{L}A_k(\mathbf{x}) = \mu_k A_k(\mathbf{x})$. The cavity modes are orthonormal with respect to the inner product in $L_2(X)$ either when the round-trip propagation inside the cavity is the same in both directions of propagation (the operator \mathcal{L} is then self-adjoint) or when the cavity is stable and does not contain apertures (in this case the modes of \mathcal{L} are Gauss-Laguerre or Gauss-Hermite functions even when \mathcal{L} is not self-adjoint). In general, the modes of a cavity with a hard or soft aperture are not orthonormal. However, the eigenfunctions B_k of \mathcal{L}^\dagger , the Hermitian conjugate of \mathcal{L} , are such that $(B_i, A_j) = \delta_{ij}$ [12].

By using the basis of the cavity modes $A_k(\mathbf{x})$ in $H_F(X)$, the basis of f_i in $H_F(T)$, and the bases $\bar{B}_k(\mathbf{x})$ and $\bar{b}_i(t)$, with $(b_i, f_j)_T = \delta_{jk}$, on their dual spaces, we find the matrix representations²

¹By taking $\psi_n \equiv \lambda_n^{-1} U \bar{\varphi}_n$ with $\mathcal{U} \bar{\varphi}_n = \lambda_n^2 \bar{\varphi}_n$, one has that $U^* \psi_n = \lambda_n \bar{\varphi}_n$. Therefore $V(\bar{\varphi}_n, \psi_n)^T = \lambda_n (\bar{\varphi}_n, \psi_n)^T$ and the functions ψ_n found in this way are orthogonal in time for the properties of V .

²The existence of the functions $b_i(t)$, which are linear combinations of the $f_i(t)$, depends on the linear independence of the $f_i(t)$. When the number m of linearly independent $f_i(t)$, i.e., the dimension of the largest invertible submatrix of \mathcal{T} , is less than the number M of A_i , one can decompose the field as $F = \sum_{i=1}^m \bar{f}_i A_i = \sum_{i=1}^m \bar{f}_i A'_i$, where the A'_i are m linear combinations of the A_i and are themselves linearly independent. One can obtain representations of $\mathcal{U}, \mathcal{U}^*$, and V with non-null submatrices of the lowest possible dimension, the square of the dimension of $H_F(X)$ and $H_F(T)$, by using m linearly independent f_i , the corresponding A'_i and their adjoint functions. Equations (15)–(17) apply with these bases.

$$\begin{aligned} (B_i, \mathcal{U} A_j)_X &= \int_X \bar{B}_i(\mathbf{x}) \left[\int_T F(\mathbf{x}, t) \int_X \bar{F}(\mathbf{x}', t) A_j(\mathbf{x}') dx' dt \right] dx \\ &= \mathcal{T}_{i,l} \mathcal{A}_{l,j} = \int_T \bar{f}_i(t) g_j(t) dt = (f_i, g_j)_T, \end{aligned} \quad (15)$$

$$(b_i, \mathcal{U}^* f_j)_T = \mathcal{A}_{i,l} \mathcal{T}_{l,j}, \quad (16)$$

$$\begin{pmatrix} 0 & (B_i, U^* f_j)_X \\ (b_i, \mathcal{U} A_j)_T & 0 \end{pmatrix} = \begin{pmatrix} 0 & \mathcal{T}_{i,j} \\ \mathcal{A}_{i,j} & 0 \end{pmatrix}, \quad (17)$$

where we have used the convention of summation over the repeated index l . \mathcal{A}_{ij} is the metric tensor of the space spanned by the cavity modes, and \mathcal{T}_{ij} is the matrix of the average amplitude products and contains information on the dynamics of the modes. The expression $\bar{g}_i(t) = (A_i, F(\mathbf{x}, t))_X$ for the amplitude of the adjoint mode B_i . Neither the functions $b_i(t)$ nor the $B_i(\mathbf{x})$ need to be found explicitly. Note that the matrix in Eq. (15) is the paraxial version of the mutual intensity matrix defined in Ref. [13]. From Eq. (15), we see that the entropy H defined by Eq. (7) or Eq. (8) can be computed using either the eigenvalues of the matrix \mathcal{T} times the metric tensor \mathcal{A} , or the eigenvalues of the temporal matrix $\langle f_i g_j \rangle_T$. On the other hand, Eq. (8) shows that it is possible to compute the entropy by decomposing the electric field on any basis. The advantage of the biorthogonal decomposition is to provide a straightforward interpretation of the entropy, as the eigenvalues λ_n^2 measure the energy of the independent modes $\varphi_n(\mathbf{x})$.

The relation between topos and chronos and cavity modes A_k and their amplitudes \bar{f}_k is given by Eq. (17). A_k are topos and f_k are chronos if and only if the two matrices $\mathcal{A}_{ij} \equiv (A_i, A_j)_X$ and $\mathcal{T}_{ij} \equiv (f_i, f_j)_T$ are both diagonal. As the matrix $\mathcal{A}_{i,j}$ is not diagonal in cavities with nonorthogonal modes, in these cavities topos and cavity modes are always different regardless of the the laser dynamics, except for the trivial case of single-mode dynamics. For cavities with orthogonal modes we need to consider the condition $\mathcal{T}_{ij} = \delta_{ij} C_j$, where the $\{C_j\}$ are normalization constants, on the average amplitude products. This condition is rarely exactly satisfied, but, from the practical point of view, what matters is how much this condition is violated for averages over long times. From Ref. [3], we expect cavity modes and their amplitudes to be a very good approximation of topos and chronos in some dynamical regimes of the laser, but not in others.

The most important aspect of these representations is that they enable us to reduce considerably the amount of information necessary to detect bifurcations in the systems. As a matter of fact, a great amount of information is provided by the matrices \mathcal{A}_{ij} and \mathcal{T}_{ij} even when the amplitudes $f_k(t)$ are not known precisely. This has important implications from the viewpoint of experimental implementation of this technique.

D. The biorthogonal decomposition, entropy, and synchronization

In Ref. [8] the biorthogonal decomposition is introduced as a tool to study the changes in symmetry of a dynamical system as a function of its control parameters, by looking at the dimensions of the eigenspaces when two or more eigenvalues of the operators U and U^* cross. While this is also possible for a laser, here we are interested in a dynamical regime, multimode dynamics driven by high pump powers, where the symmetry of the laser is completely broken, i.e., the laser solutions do not display any spatial or temporal symmetry. We want to determine what can produce significant variations to the coupling of the topos with the pump, as well as the spatial coherence and the entropy of the systems. We show here that these changes are in general not caused by eigenvalues crossing, but by the appearance at a value $\chi_0 + \Delta\chi$ of the pump of off-diagonal terms in the matrix \mathcal{T} of the amplitudes of the topos, $\varphi(\mathbf{x}'; \chi_0)$, found at value χ_0 . These terms, in turn, are caused by the appearance (or disappearance) of synchronization; we also introduce in the following the tools to detect them.

1. Eigenvalues crossing with null off-diagonal matrix elements

This happens when the energies of two $\varphi_i(\mathbf{x}; \chi_0)$ change, but their dynamics are incoherent. As a consequence, the structure of the topos are the same before and after the eigenvalue crossing. As the average coupling with the pump of the topos is mainly due to its shape, the rate of variation of their energy as a function of the control parameters is largely unaffected by the crossing. It is not possible to predict the effect of this type of transition on the entropy, but in our simulations this effect is very small.

2. Complete synchronization of two or more amplitudes

In this case the amplitudes of two or more elements of the basis $\varphi_i(\mathbf{x}; \chi_0)$ are proportional. The number of synchronized elements is given by the difference between the dimension of the largest invertible minor of \mathcal{T} at $\chi_0 + \Delta\chi$ and at χ_0 . This type of synchronization reduces the maximum possible value of $H, \log M$. The actual value of H can also be reduced, depending on the relative position of the eigenvalues of \mathcal{U} .

3. Off-diagonal elements of \mathcal{T} and phase synchronization of chaotic amplitudes

Consider first the case of two basis elements for which two off-diagonal elements appear in the matrix \mathcal{T} as the control parameters are changed. The size of the off-diagonal elements and their effect is significant if the two amplitudes are synchronized in phase for most of the time, otherwise it is negligible. The off-diagonal terms increase the separation of the eigenvalues of \mathcal{U} corresponding to the two coupled modes.³ This will also result in a variation of the structure of

³The separation between the eigenvalues of \mathcal{U} is $\Delta\lambda = [(\mathcal{U}_{11} + \mathcal{U}_{22})^2 + 4|\mathcal{U}_{12}|^2]^{1/2}$, where we have ordered the $\varphi_i(\mathbf{x}; \mathbf{P}_0)$ so that the first two are the coupled ones.

two basis elements and, therefore, in a change in the rate of variation of energy versus the pump. This can be detected by tracking the eigenvalues of \mathcal{U} . Depending on the positions of these two eigenvalues, the gap between the eigenvalues can reduce the value of the entropy H defined in Eq. (7).

This result can be generalized to the case of N uncoupled basis elements that become coupled to a $(N+1)$ th element [[14], pp. 37–42]. As in the previous case, synchronization between a basis function and a set of other basis functions produces a sudden increase in the energy separation between the lowest and the highest of the corresponding eigenvalues.⁴ Furthermore, the spatial structure of all the coupled topos changes. Again, this will show as a variation of the rate of change of the corresponding eigenvalues. Depending on the position of the set, the gap in the distribution of eigenvalues caused by synchronization may reduce the values of the entropy H , as we have observed numerically.

4. Uncorrelated entropy

For the previous two cases we have used exact results from the theory of Hermitian matrices. More general couplings can be analyzed using Gershgorin's theorem. This states that the eigenvalues of an arbitrary $n \times n$ matrix a_{ij} lie in the region of the complex z plane consisting of n disks having for centers the diagonal matrix elements a_{ii} and for radii the sum of the moduli of the off-diagonal elements of the matrix rows, $\sum_{j=1, j \neq i}^n |a_{ij}|$. From Eq. (15), the centers and the corresponding radii of the Gershgorin disks for \mathcal{U} are given, respectively, by

$$z_k = \mathcal{T}_{k,l} \mathcal{A}_{l,k} = (f_k, g_k)_T, \tag{18}$$

$$\rho_k = \sum_{j \neq k} |\mathcal{T}_{k,l} \mathcal{A}_{l,j}| = \sum_{j \neq k} |(f_k, g_j)_T|. \tag{19}$$

From these equations we can conclude that in the absence of synchronization between the cavity modes, i.e., if $|(f_k, f_j)_T| \ll 1$ when $j \neq k$, the Gershgorin radii are very small: as a consequence the eigenvalues of the biorthogonal decomposition are proportional to the intensity of the cavity modes and the topos can be identified with the cavity modes. Therefore, we can assess the importance of the average products by comparing H with the uncorrelated entropy

$$H_0 = - \sum_n p_n^{(0)} \log(p_n^{(0)}), \tag{20}$$

where

⁴In this case eigenvalues of \mathcal{U} are given by $\sum_{i=1}^N |\mathcal{U}_{i,N+1}|^2 / (\lambda - \lambda_i^0) = \lambda - \mathcal{U}_{N+1,N+1}$, where λ_i^0 are the eigenvalues of the submatrix of \mathcal{U} over the first N modes. If there are n λ_i^0 below $\mathcal{U}_{N+1,N+1}$, the order of the eigenvalues of \mathcal{U} is $\lambda_1 < \lambda_1^0 < \lambda_2 < \lambda_2^0 < \dots < \lambda_{m-1} < \lambda_m^0$ and $\lambda_{m+1}^0 < \lambda_{m+2} < \lambda_{m+2}^0 < \dots < \lambda_N^0 < \lambda_{N+1}$, with $\lambda_m^0 < \lambda_{m+1} < \mathcal{U}_{N+1,N+1}$ if $\sum_{i=1}^n |\mathcal{U}_{i,N+1}|^2 / (\lambda - \lambda_i^0) < \sum_{i=n+1}^N |\mathcal{U}_{i,N+1}|^2 / (\lambda - \lambda_i^0)$ or $\mathcal{U}_{N+1,N+1} < \lambda_{m+1} < \lambda_{m+1}^0$ if $\sum_{i=1}^n |\mathcal{U}_{i,N+1}|^2 / (\lambda - \lambda_i^0) > \sum_{i=n+1}^N |\mathcal{U}_{i,N+1}|^2 / (\lambda - \lambda_i^0)$.

$$p_n^{(0)} = \frac{(f_n, f_n)_T (A_n, A_n)_X}{\sum_j (f_j, f_j)_T (A_j, A_j)_X}$$

is the normalized energy of the n th cavity mode.

E. Applications to experiments

The most interesting aspect of this techniques is that it is not necessary to measure the amplitude and phase of the electric field, it is enough to determine the matrix \mathcal{T} of time averages of amplitude products. This matrix can be determined just by average intensity measurements.

For a convenient basis of known functions $s_j(\mathbf{x})$ (not necessarily the cavity modes), with amplitudes $v_i(t)$, we need to measure the matrix $\mathcal{T}_{ij} = (v_i, v_j)_T$. This can be done by measuring the average intensity of the laser

$$\langle |F(\mathbf{x}, t)|^2 \rangle_T = \frac{1}{T} \int_0^T |F(\mathbf{x}, t)|^2 dt = \sum_{i,j} \langle v_i \bar{v}_j \rangle_T s_i(\mathbf{x}) \bar{s}_j(\mathbf{x}). \quad (21)$$

Let \mathbf{x}_m , with $m = 1, \dots, M^2$, be a set of points in the transverse plane of the laser and let $K_{ij}^{(m)} \equiv s_i(\mathbf{x}) \bar{s}_j(\mathbf{x})$. We can rewrite Eq. (21) as a linear system of M^2 equations for the unknown average products $\langle v_i \bar{v}_j \rangle_T$:

$$\sum_{i,j} K_{ij}^{(m)} \langle v_i \bar{v}_j \rangle_T = \langle |F(\mathbf{x}_m, t)|^2 \rangle_T, \quad m = 1, 2, \dots, M^2. \quad (22)$$

The solution of this system can then be used in Eqs. (14) and (15) to determine the topos and their corresponding eigenvalues. The functions s_i and the points \mathbf{x}_m should be chosen so that the system (22) is well-conditioned [15]. The number M of functions s_i necessary should be determined through a least squares procedure from the fitting of the average intensity patterns. Moreover, it may be computationally advantageous to measure the average intensity in more than M^2 points and use a least squares procedure to determine the average amplitude products.

The information provided by the matrices \mathcal{T} and \mathcal{A} can be complemented by the fast Fourier transform (FFT) of the signal from a few fast detectors placed in points of the beam. This is particularly useful in case of synchronization. Peaks of the FFT are caused by the beating of modes with different frequency. Reduction in the number of peaks indicates synchronization. By measuring the FFT of the beating of the multimode beam with a single-mode reference beam, one could detect not only the synchronization of modes, but also the position of the central frequency of the synchronized modes.

III. ENTROPY OF MULTIMODE LASER DYNAMICS

We have used the tools described in the previous section to analyze the multimode dynamics of the laser modeled by Eqs. (9)–(11). The model and numerical procedure used are described in [3]. For the purpose of this paper, we have chosen a variety of slightly astigmatic cavities with intracavity aperture. They were described by two sets of $ABCD$ matri-

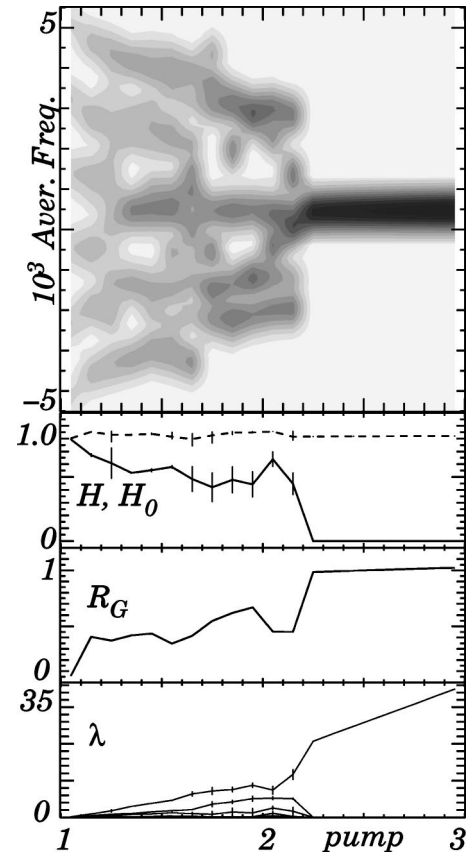


FIG. 1. See text. Cavity parameters: $A_x = D_x = 0.506$; $B_x = -0.280$; $A_y = D_y = 0.508$; $B_y = -0.280$; radius of the intracavity aperture, three beam waists. Laser parameters: $\gamma = 0.1$; cavity round-trip time equal to the polarization decay time, 6% losses per round trip; atom-cavity detuning, 0.05; flat pump; integration time, 16384 round-trips.

ces, one per coordinate axis in the transverse plane: the effect of the astigmatism is to remove the frequency degeneracy of the cavity modes belonging to the same family. The choice of different cavities has allowed us to control the number of modes that play a role in the dynamics of the laser. For each cavity configuration we have run two batches of simulations for two different values of γ , $\gamma = \{0.1, 0.025\}$. Each batch consisted of 100 simulations for 20 different values of the pump parameter $\chi = 1.05, 1.15, \dots, 2.95$, and for five sets of different initial condition per pump value.

The analysis of some of the simulations is summarized in Figs. 1–5. For each batch of simulations we have computed the following.

(1) The average frequency of each cavity mode (top plot). This has been computed as the ratio between the difference of the final from the initial phase of each mode and the integration time. For each value of the pump the frequencies obtained from the five simulations corresponding to different initial conditions are plotted as smooth histograms [16]. The final result is a contour plot whose coordinates are the pump and the average frequency: this plot clearly shows whether synchronization, defined as two or modes evolving with the same average frequency, takes place. The shading of the plot is proportional to the energy in the given frequency

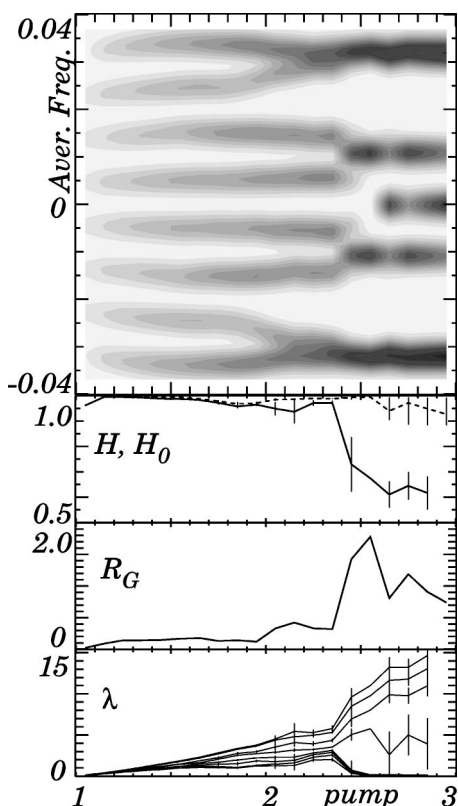


FIG. 2. See text. Cavity parameters: $A_x=D_x=0.925$; $B_x=0.025$; $A_y=D_y=0.921$; $B_y=0.026$; radius of the intracavity aperture, three and half beam waists. Laser parameters: as in Fig. 1 except $\gamma=0.025$; atom-cavity detuning, 0.021; integration time 65 536 round-trips.

band (inverted gray scale; bright, no energy; dark, most energy). A similar plot could be obtained from experimentally measured temporal power spectra.

(2) The entropy H and the uncorrelated entropy H_0 (second plot). For each value of the pump we have plotted the average entropy of the five simulations with different initial conditions. The error bars indicate the rms variation of the entropies. In each plot we have scaled the entropy with $\log(M)$, with M the number of modes included in the simulation in order to ensure that the range of the entropy is between 0 and 1.

(3) The scaled average Gershgorin radius R_G (third plot). This has been computed by determining the average of the radii ρ_k given by Eq. (19) and scaling it with the average distance between the center of the Gershgorin circles, Eq. (18). This scaled radius indicates whether synchronization is strong enough to move the eigenvalues of the biorthogonal decomposition significantly away from the average intensity of the cavity modes.

(4) The eigenvalues of the biorthogonal decomposition, λ (bottom plot). For each value of the pump we have plotted the average eigenvalues of the five simulations with different initial conditions. The error bars indicate the rms variation of the eigenvalues.

When only few modes are active (Fig. 1) we observe complete synchronization at high pump power: only one topos has eigenvalue different from zero. The entropy drops to

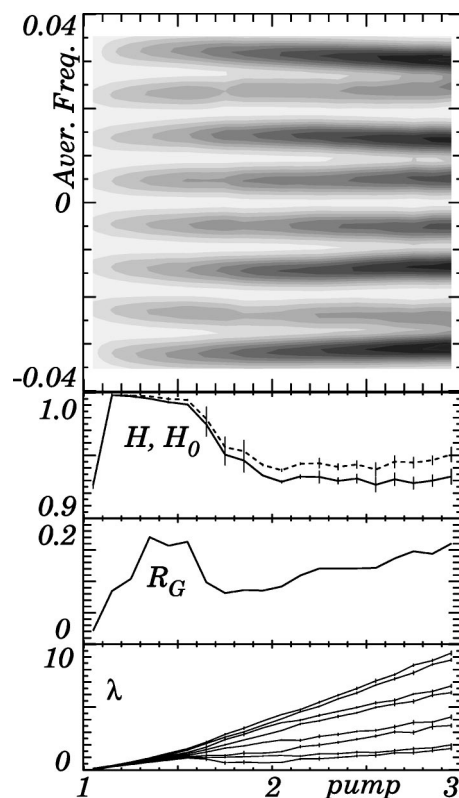


FIG. 3. See text. Cavity parameters: As in Fig. 2. Laser parameters: as in Fig. 2 except $\gamma=0.1$.

zero, but not the uncorrelated entropy. When the two entropies are significantly different, the scaled Gershgorin radius is of the order of unity. This is exactly the same scenario as the two-mode cavity analyzed in [1]. If the number of modes is increased (Fig. 2) we observe only partial synchronization, but the behavior of the entropy is still qualitatively similar to the previous case: it first increases and then decreases as the dynamics settles in a smaller number of coherent structures. At the onset of synchronization there is an abrupt change of the rate of variation of the eigenvalues with the pump and all the energy is contained within four topos. From the plot of the average frequency we see that modes that are frequency locked have quite close natural frequencies. However, the natural frequency alone does not explain why some modes are locked and other not. Moreover, increasing γ , i.e., increasing the rate of evolution of the population inversion, makes it harder for the modes to synchronize and reduces the decrease in entropy (see Fig. 3). This is also confirmed by the graphs of the eigenvalues (compare Fig. 2 with Fig. 3).

The situation in Figs. 2 and 3 is somewhat artificial: there are neighboring families of modes that have not been included in the numerical simulation. If we include them, as in Fig. 4 we see that the situation becomes more complicated: as the pump parameter is increased modes that are further away from the center of the gain line become active and the entropy never decreases, even though it remains smaller than the uncorrelated entropy. Moreover, the appearance of active high-energy modes at different frequencies seems to disrupt the synchronization of the modes in the central family and only the most energetic topos, i.e., the one with largest ei-

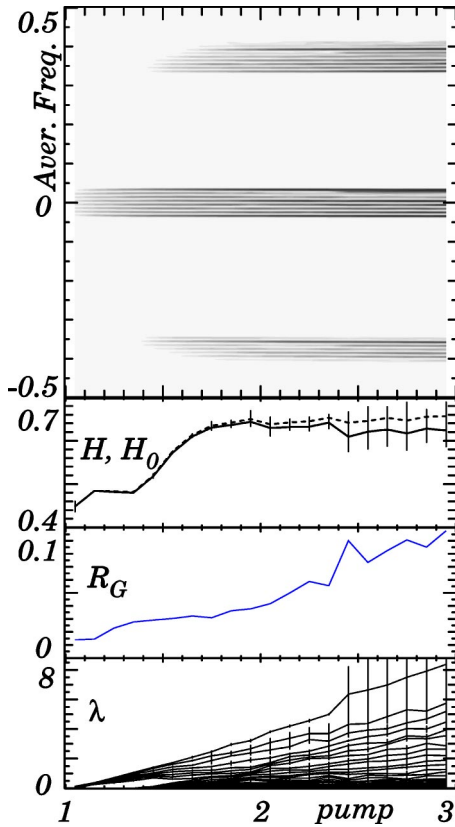


FIG. 4. See text. Cavity parameters: as in Fig. 2. Laser parameters: as in Fig. 2, but the 72 most resonant modes with smallest losses were included in these simulations.

genvalue, shows any sudden change in slope.

The inclusion of a finite-width pump produces rather significant changes in the behavior of the entropy. The case in Fig. 5 illustrates this case: as in the previous figure there are two neighboring families of modes that become active as the pump is increased. However, they are wider than the central family and have a smaller overlap with the finite width pump. They therefore do not disrupt the synchronization of the modes in the central family and the entropy decreases. In this final case the variation in the rate of change of the largest eigenvalue at the onset of synchronization is quite remarkable.

IV. CONCLUSIONS

The biorthogonal decomposition, based on the spatial- and time-average properties of the dynamics, is a powerful tool to understand and characterize the seemingly featureless turbulent dynamics of multimode lasers. In particular, the study of the structure of the time-average product matrix \mathcal{T} in Sec. II D shows how the interaction between modes as the pump power is increased can reduce the complexity of the laser dynamics and enhance its spatial coherence. As we have shown in Sec. III we expect this to happen under very realistic assumptions, e.g., that the pump width is finite. This is a surprising result that goes counter to the “natural expectation” that the dynamics of the laser would become more complex at higher power.

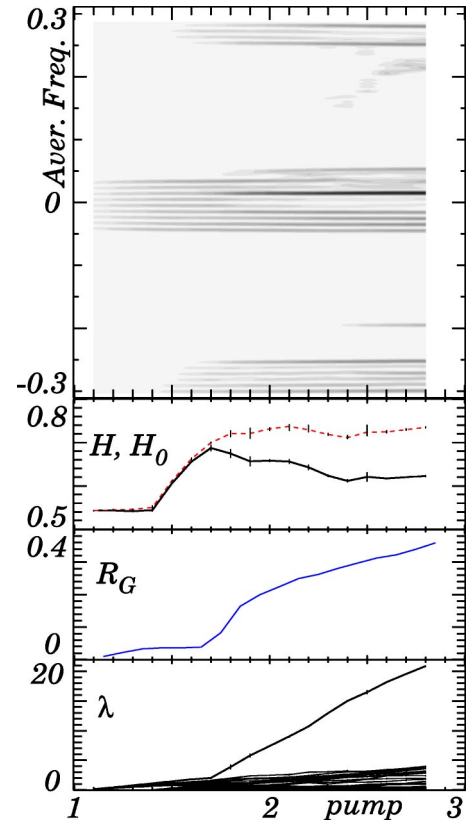


FIG. 5. See text. Cavity parameters: as in Fig. 2, except radius of the intracavity aperture, 5.1 beam waists. Laser parameters: as in Fig. 1, except atom-cavity detuning -2.72 ; super-Gaussian pump of width 7 beam waists; integration time, 30 000 round trips; $\chi = \{1.1, 1.2, \dots, 2.8\}$; the 56 most resonant modes with smallest losses were included in this simulation.

Even though in this paper we have analyzed the results of numerical simulations, the biorthogonal decomposition is also an experimental tool. As the matrices \mathcal{A} and \mathcal{T} are averages over either space or time, it is possible to measure them without the use of fast detectors: this is of paramount importance in optics where the time scales are extremely short and it opens the possibility to characterize experimentally the spatiotemporal dynamics of, for example, fast semiconductor lasers. Moreover, the information contained in the average matrices \mathcal{A} and \mathcal{T} can be complemented by the Fourier transform of the signal intensity or of its heterodyne at a few points, thus obtaining a fairly broad and detailed knowledge of the laser dynamics.

Underlying the results of this paper is the open question of why some modes synchronize and others do not. Our numerical analysis suggests that the answer has many facets and the synchronization depends on spatial characteristics of the modes, e.g., the overlap between modes and pump and other modes, and on their temporal properties, e.g., their natural frequency. The answer to this question coupled to the results of this paper would allow us not only to determine *a posteriori* the complexity of the laser dynamics, but also to predict its behavior and, ultimately, control it.

- [1] D. R. J. Chillingworth, G. D'Alessandro, and F. Papoff, *Physica D* **177**, 175 (2003).
- [2] A. G. Vladimirov, E. A. Viktorov, and P. Mandel, *Phys. Rev. E* **60**, 1616 (1999).
- [3] G. D'Alessandro, F. Papoff, E. Louvergneaux, and P. Glorieux, *Phys. Rev. E* **69**, 066212(11) (2004).
- [4] P. Kolodner, S. Slimani, N. Aubry, and R. Lima, *Physica D* **85**, 165 (1995).
- [5] D. Dangoisse, D. Hennequin, C. Lepers, E. Louvergneaux, and P. Glorieux, *Phys. Rev. A* **46**, 5955 (1992).
- [6] E. Louvergneaux, D. Hennequin, D. Dangoisse, and P. Glorieux, *Phys. Rev. A* **53**, 4435 (1996).
- [7] Y. F. Chen and Y. P. Lan, *Phys. Rev. A* **65**, 013802 (2002).
- [8] N. Aubry and R. Lima, *J. Stat. Phys.* **81**, 793 (1995).
- [9] N. Aubry, R. Guyonnet, and R. Lima, *J. Stat. Phys.* **67**, 183 (1992).
- [10] N. Aubry, R. Guyonnet, and R. Lima, *J. Stat. Phys.* **64**, 683 (1991).
- [11] J. Von Neumann, *Mathematical Foundations of Quantum Mechanics* (Princeton University Press, Princeton, NJ, 1955).
- [12] A. E. Siegman, *Lasers* (University Science, Mill Valley, CA, 1986).
- [13] H. Gamo, *Prog. Opt.* **3**, 187 (1964).
- [14] E. U. Condon and G. H. Shortley, *The Theory of Atomic Spectra* (Cambridge University Press, London, 1935).
- [15] G. H. Golub and V. C. F., *Matrix Computations*, 3rd ed. (Johns Hopkins University Press, Baltimore, 1996).
- [16] E. Parzen, *Ann. Math. Stat.* **33**, 1065 (1962).